

Scalar field evolution in Gauss-Bonnet black holes

E. Abdalla* and R.A. Konoplya†
Instituto de Física, Universidade de São Paulo
C.P. 66318, 05315-970, São Paulo-SP, Brazil

C. Molina‡
Escola de Artes, Ciências e Humanidades, Universidade de São Paulo
Av. Arlindo Bettio 1000, CEP 05315, São Paulo-SP, Brazil

We present thorough analysis of scalar perturbations in the background of Gauss-Bonnet, Gauss-Bonnet-de Sitter and Gauss-Bonnet-anti-de Sitter black hole spacetimes. The perturbations are considered both in frequency and time domain. The scalar field evolution is crucially dependent on the values of the cosmological constant and the Gauss-Bonnet coupling. For Gauss-Bonnet and Gauss-Bonnet-de Sitter black holes, at asymptotically late times either power-law or exponential tails are dominating, while for Gauss-Bonnet-anti-de Sitter black hole, the quasinormal modes govern the scalar field decay at all times. For the limit of near extremal value of the (positive) cosmological constant and pure de Sitter and anti-de Sitter modes in Gauss-Bonnet gravity we have found analytical expressions.

PACS numbers: 04.30.Nk, 04.50.+h

I. INTRODUCTION

Black holes in more than four spacetime dimensions are of considerable interest recently due to the two main reasons: they naturally appear in string theory, and in extra dimensional brane-world scenarios [1]. According to some of these scenarios it is possible that the small higher dimensional black holes can be produced in particles collisions in Large Hadron Collider. At the same time quantum gravity may show itself already at TeV-energy scale. Yet, the effects of quantum gravity then may be observed as corrections to classical General Relativity.

String theory predicts quantum corrections to classical General Relativity, and the Gauss-Bonnet terms is the first and dominating correction among the others. Several higher other theories of gravity sustain black hole solutions. Boulware and Deser [2], as well as Wheeler [3] discovered black hole solutions in Gauss-Bonnet gravity. More generally, Lovelock gravity [4] has been studied and shown to possess black hole solutions with interesting thermodynamical properties [5, 6].

Here we consider quasinormal perturbations of Gauss-Bonnet black holes including a non-vanishing cosmological constant. Quasinormal modes are a very useful tool to uncover properties of the intrinsic geometry, since the modes characterizes well the geometry and does not depend on further extrinsic properties, independent of the geometry itself [7]. They have been used successfully in a large class of astrophysical questions, from black holes to stars. In addition, it has been argued that the Gauss-Bonnet gravity in asymptotically anti-de Sitter

(AdS) spacetimes may be analyzed through anti-de Sitter/conformal field theory (AdS/CFT) correspondence within next-to-leading order [8]. In this case the quasinormal modes of the large Gauss-Bonnet-AdS black hole could find a holographic interpretation in conformal field theory, as is the cases for the AdS black hole in Einstein gravity [9].

In [10] the quasinormal modes for a charged asymptotically flat black hole in Gauss-Bonnet gravity were found with the help of the WKB approach [11]. The asymptotically high overtone behavior of the spectrum has been discussed recently in [12], and the tensor-type of gravitational perturbations in [13].

The quasinormal modes are obtained using numerical analysis as well as a semi-analytical WKB-type treatment. Such an approach is based on the fact that the wave equation is similar to a Schrödinger equation, and depending on the kind of potential, it makes sense to borrow the methods used in quantum mechanics in order to define a semi-classical approximation. This vein has been followed and an approximation for the quasinormal frequencies has been obtained to a high WKB order [11]. In addition to the frequency domain, we analyze the evolution of scalar perturbations in the time domain and find good agreement between the results found by the two approaches.

The paper is organized as follows: Sec. II represents the preliminaries of the Gauss-Bonnet-(A)dS metric and its scalar perturbations. Sec. III is devoted to the methods used in the paper, namely the WKB method (in the frequency domain), and the characteristic integration method (in the time domain). Sec. IV discuss the quasinormal behavior of the Gauss-Bonnet (GB), Gauss-Bonnet-de Sitter (GBdS) and Gauss-Bonnet-anti-de Sitter (GBAdS) black holes. In Sec. V we discuss the future perspective and unsolved questions in this field.

*Electronic address: eabdalla@fma.if.usp.br

†Electronic address: konoplya@fma.if.usp.br

‡Electronic address: cmolina@usp.br

II. GAUSS-BONNET BLACK HOLE SOLUTIONS

The Einstein-Gauss-Bonnet action is given by

$$S = \int \sqrt{-g} \left[\frac{1}{2\alpha^2} (R - 2\Lambda + \alpha \mathcal{L}_{GB}) \right] d^d x \quad , \quad (1)$$

where R and Λ are the d -dimensional Ricci scalar and the cosmological constant, respectively. The parameter α represents the Gauss-Bonnet coupling constant.

The Gauss-Bonnet Lagrangian \mathcal{L}_{GB} is given by

$$\mathcal{L}_{GB} = R^2 - 4R_{\mu\nu}R^{\mu\nu} + R_{\mu\nu\rho\sigma}R^{\mu\nu\rho\sigma} \quad . \quad (2)$$

One should note that in four dimensions the Gauss-Bonnet term (2) is a total divergency, and yields upon integration a topological invariant, namely the genus of the hypersurface defining the Gauss-Bonnet action.

A metric obtained as a solution of the field equations is given by

$$ds^2 = -h(r)dt^2 + h(r)^{-1}dr^2 + r^2 d\Omega_{d-2}^2 \quad , \quad (3)$$

where the function $h(r)$ is given by the expression

$$h(r) = 1 + \frac{r^2}{2\alpha} - \frac{r^2}{2\alpha} \sqrt{1 + \frac{8\alpha\mu}{r^{d-1}} + \frac{8\alpha\Lambda}{(d-1)(d-2)}} \quad . \quad (4)$$

The constant μ is proportional to the black hole mass and $d\Omega_{d-2}^2$ is the line element of the $(d-2)$ -dimensional unit sphere.

We set up a scalar field Φ on such a background obeying the Klein-Gordon equation

$$\square\Phi = \frac{1}{\sqrt{-g}}\partial_\mu(\sqrt{-g}g^{\mu\nu}\partial_\nu\Phi) = 0 \quad . \quad (5)$$

In order to separate the wave function in terms of eigenpotential we first separate the variables as $\Phi(t, r, \{\theta_i\}) = R_\ell(t, r)Y_{\ell m}(\{\theta_i\})/r$. As usual we obtain a simple equation for $R_\ell(t, r)$, which is given by the expression

$$4\frac{\partial^2 R_\ell(u, v)}{\partial u \partial v} + V(r(u, v))R_\ell(u, v) = 0 \quad (6)$$

where $u = t - r_\star$, $v = t + r_\star$ and the tortoise coordinate r_\star is defined by the relation

$$\frac{dr_\star}{dr} = \frac{1}{h(r)} \quad . \quad (7)$$

The variables u and v are the light cone coordinates corresponding to the time and tortoise coordinate. The effective potential for the scalar field in (6) is

$$V(r) = h(r) \left[\frac{(d-2)(d-4)}{4r^2} + \frac{d-2}{2r}h'(r) + \frac{\ell(\ell+d-3)}{r^2} \right] \quad . \quad (8)$$

III. NUMERICAL AND SEMI-ANALYTICAL APPROACHES

A. Characteristic integration

In [14] a simple but very efficient way of dealing with two-dimensional d'Alembertians has been set up. Along the general lines of the pioneering work [15], light-cone variables have been introduced as above, leading to (6).

In the characteristic initial value problem, initial data are specified on the two null surfaces $u = u_0$ and $v = v_0$. The basic aspects of the field decay are independent of the initial conditions (as confirmed by simulations), so we use Gaussian initial conditions.

Since we do not have analytic solutions to the time-dependent wave equation with the effective potentials introduced, one approach is to discretize the equation (6), and then implement a finite differencing scheme to solve it numerically. One possible discretization, used for example in [16, 17, 18], is

$$R_\ell(N) = R_\ell(W) + R_\ell(E) - R_\ell(S) - \Delta^2 V(S) \frac{R_\ell(W) + R_\ell(E)}{8} \quad , \quad (9)$$

where we have used the definitions for the points: $N = (u + \Delta, v + \Delta)$, $W = (u + \Delta, v)$, $E = (u, v + \Delta)$ and $S = (u, v)$. Another possible scheme is

$$\left[1 - \frac{\Delta^2}{16} V(S) \right] R_\ell(N) = R_\ell(E) + R_\ell(W) - R_\ell(S) - \frac{\Delta^2}{16} [V(S)R_\ell(S) + V(E)R_\ell(E) + V(W)R_\ell(W)] \quad . \quad (10)$$

Although the second discretization (10) is more time consuming than (9), it was observed in [19] that (10) is more stable for fields in asymptotically AdS geometries. With the use of expression (9) or (10), the basic algorithm will cover the region of interest in the $u - v$ plane, using the value of the field at three points in order to calculate it at a forth one. After the integration is completed, the values of R_ℓ in the regions of interest are extracted.

B. WKB analysis

Considering the Laplace transformation of the eq. (6) (in terms of t and r_\star), one gets the ordinary differential equation

$$\frac{d^2 \psi_\ell(r_\star)}{dr_\star^2} - [s^2 + V(r_\star)] \psi_\ell(r_\star) = 0 \quad . \quad (11)$$

One finds that there is a discrete set of possible values of s such that the function $\psi_\ell(r_\star)$ satisfies both boundary conditions:

$$\lim_{r_\star \rightarrow -\infty} \psi_\ell e^{sr_\star} = 1, \quad (12)$$

$$\lim_{r_\star \rightarrow +\infty} \psi_\ell e^{-sr_\star} = 1. \quad (13)$$

By making the formal replacement $s = i\omega$, we have the usual quasinormal mode boundary conditions. The frequencies ω (or s) are the quasinormal frequencies.

The semi-analytic approach used in this work [11] is a very efficient algorithm to calculate the quasinormal frequencies, which have been applied in a variety of situations [20].

Under the choice of the positive sign of the real part of ω ($\omega = \text{Re}(\omega) + i\text{Im}(\omega)$), QNMs of Gauss-Bonnet and Gauss-Bonnet-de Sitter black holes satisfy the following boundary conditions

$$\psi(r_\star) \propto C_\pm \exp(\pm i\omega r_\star), \quad r_\star \rightarrow \pm\infty, \quad (14)$$

corresponding to purely in-going waves at the event horizon and purely out-going waves at null infinity (or cosmological horizon, if $\Lambda > 0$). For the Gauss-Bonnet-anti-de Sitter geometries, the effective potential is divergent at spatial infinity (which corresponds to a finite value of r_\star , here taken as 0). In the present work, we assume Dirichlet boundary conditions, setting $\psi_\ell(r_\star = 0) = 0$.

To find the quasinormal modes of the black hole whose effective potential has the form of a potential barrier (GB and GBdS black holes) one can use a high order WKB approach, finding

$$i \frac{\omega^2 - V_0}{\sqrt{-2V_0''}} - L_2 - L_3 - L_4 - L_5 - L_6 = n + \frac{1}{2}, \quad (15)$$

where V_0 is the height and V_0'' is the second derivative with respect to the tortoise coordinate of the potential at the maximum. L_2, L_3, L_4, L_5 and L_6 are presented in [11]. Thus we are able to use this formula for finding the quasinormal modes of Gauss-Bonnet and Gauss-Bonnet de Sitter black holes. Yet, for Gauss-Bonnet anti-de Sitter it cannot be applied as the corresponding potential is divergent at spatial infinity.

IV. EVOLUTION OF PERTURBATIONS: TIME AND FREQUENCY DOMAIN

In this section we shall discuss the quasinormal and late-time behavior for scalar field perturbations in the exterior of Gauss-Bonnet black holes, generally, with a null, positive and negative Λ -term, and therefore one has to consider the correlation of the scalar field evolution with “global” parameters: GB-coupling α , Λ -term, space-time dimensionality, and “local” parameters such as black hole mass μ and multipole number ℓ .

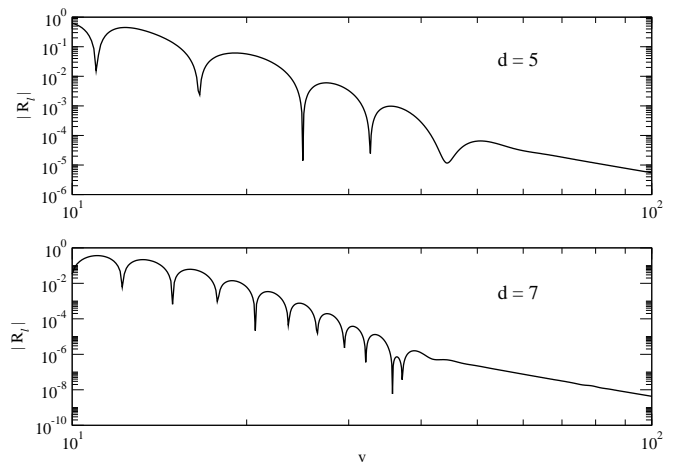


Figure 1: Field decay in the Gauss-Bonnet black holes, for $d = 5$ and $d = 7$. It is observed a quasinormal mode dominated region. Asymptotically, the field decays as a power-law tail. The parameters in this graph are $\alpha = 0.1$, $\mu = 1.0$ and $\ell = 0$.

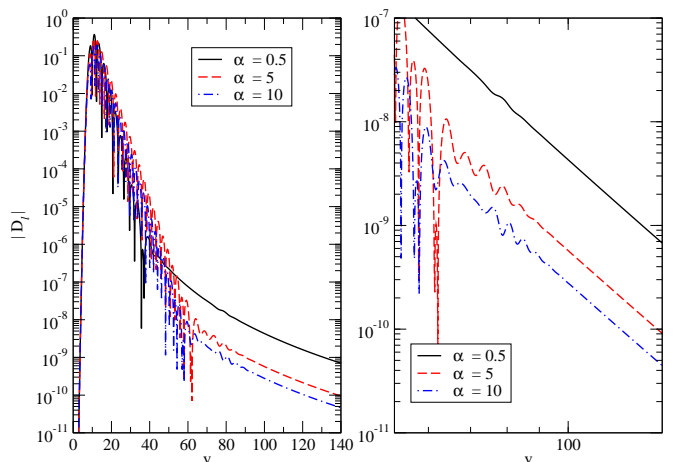


Figure 2: Power-law tails in the Gauss-Bonnet black holes. For the curves presented, the estimated power-law coefficients are the same up to a difference under 1%. The parameters in this graph are $d = 7$, $\mu = 1.0$ and $\ell = 0$.

A. Gauss-Bonnet black holes

As seen in a previous work [10], the WKB method allows very accurate calculations of the quasinormal modes associated with the field evolution. A complementary analysis can be performed within the time-dependent picture. For this purpose, we use here a characteristic initial value algorithm.

The scenario presented by the WKB calculations is consistent with the results obtained with time evolution approach. From the wave-functions calculated with the characteristic integration routine, it is observed that, after an initial transient phase, the decay is dominated by the quasinormal mode ringing. It is possible to estimate with high precision the oscillatory and exponential decay

Table I: Values for the quasinormal frequencies for the fundamental mode in the Gauss-Bonnet geometry, obtained from sixth order WKB method and directly from characteristic data, for $d = 5$, $\ell = 0, 1$ and several values of α .

$d = 5$		WKB (6th order)		Characteristic Integration	
ℓ	α	$\text{Re}(\omega_0)$	$-\text{Im}(\omega_0)$	$\text{Re}(\omega_0)$	$-\text{Im}(\omega_0)$
0	0.1	0.389935	0.256159	0.379	0.282
0	0.2	0.396034	0.250548	0.383	0.272
0	0.5	0.429741	0.208293	0.391	0.246
1	0.1	0.720423	0.255506	0.7234	0.250
1	0.2	0.723177	0.252684	0.7284	0.245
1	0.5	0.739205	0.236885	0.7443	0.228

parameters using a non-linear fitting based in a χ^2 analysis. We emphasize that the numerical concordance is excellent, as seen in Tables I - IV. The results, as compared between WKB approximation and characteristic integration agree to an accuracy between 1% and 10%. This small difference must exist, because we compare the data for the fundamental overtones in frequency domain with time domain data where the contribution from all overtones are taken into consideration. The imaginary part of the frequency does not show too much dependence on α , yet slightly decrease when α is increasing. On the other hand, the real part increases with α , though not significantly either. This might be showing that a quasinormal mode is much more an effect connected with the local geometry containing the black hole rather than with the global effect of the geometry, namely, the effect of the existence of an event horizon matters much more than a detailed dependence on the parameter α . Yet large enough values of α certainly affect the quasinormal spectrum: the QNMs are proportional to α in the regime of large α [10]. As α approaches zero, the QNMs go to those of ordinary d -dimensional Schwarzschild black hole described by the Tangerlini metric.

In the time domain the signal has three stages: the initial pulse dependent on the source of perturbations, the quasinormal ringing dominating period, and the power-law tail (see Fig.1). The bigger GB-coupling is, the larger the quasinormal dominated region, i.e. at a later times the tails start dominating. The power-law tails do not show dependence on the Gauss-Bonnet coupling α (see Fig.2).

Generally, the WKB technique shows good convergence, yet, the worse convergence of the WKB method takes place when we deal with the intermediate values of $\alpha \approx 1$. That is why, in this regime, the agreement between the WKB and the characteristic integration results is the worst.

Table II: Values for the quasinormal frequencies for the fundamental mode in the Gauss-Bonnet geometry, obtained from sixth order WKB method and directly from characteristic data, for $d = 6$, $\ell = 0, 1$ and several values of α .

$d = 6$		WKB (6th order)		Characteristic Integration	
ℓ	α	$\text{Re}(\omega_0)$	$-\text{Im}(\omega_0)$	$\text{Re}(\omega_0)$	$-\text{Im}(\omega_0)$
0	0.1	0.735854	0.402416	0.7109	0.412
0	0.2	0.748053	0.391049	0.7144	0.402
0	0.5	0.83530	0.304837	0.7225	0.375
0	5	0.906661	0.144820	0.9526	0.226
0	10	1.513624	0.456935	1.5182	0.423
0	20	2.961675	0.927128	2.878	0.952
1	0.1	1.139007	0.415034	1.153	0.395
1	0.2	1.136193	0.415706	1.159	0.386
1	0.5	1.158635	0.391339	1.176	0.363
1	5	1.790103	0.258382	1.791	0.253
1	10	3.260415	0.498426	3.253	0.504
1	20	6.437139	0.991374	-	-

Table III: Values for the quasinormal frequencies for the fundamental mode in the Gauss-Bonnet geometry, obtained from sixth order WKB method and directly from characteristic data, for $d = 7$, $\ell = 0$ and several values of α .

$d = 7$		WKB (6th order)		Characteristic Integration	
ℓ	α	$\text{Re}(\omega_0)$	$-\text{Im}(\omega_0)$	$\text{Re}(\omega_0)$	$-\text{Im}(\omega_0)$
0	0.1	1.11738	0.546056	1.092	0.532
0	0.2	1.13699	0.529543	1.092	0.520
0	0.5	1.29469	0.395111	1.092	0.493
0	5	1.39823	0.574472	1.275	0.351
0	10	1.48053	0.385616	1.515	0.358
0	20	2.00368	0.56458	2.001	0.567

B. Gauss-Bonnet-de Sitter black holes

For the GBdS black holes the quasinormal ringing stage becomes correlated with a new parameter: a positive Λ -term. When the Λ -term is growing, both real oscillation frequency and the damping rate are decreas-

Table IV: Values for the quasinormal frequencies for the fundamental mode in the Gauss-Bonnet geometry, obtained from sixth order WKB method and directly from characteristic data, for $d = 8$, $\ell = 0$ and several values of α .

$d = 8$		WKB (6th order)		Characteristic Integration	
ℓ	α	$\text{Re}(\omega_0)$	$-\text{Im}(\omega_0)$	$\text{Re}(\omega_0)$	$-\text{Im}(\omega_0)$
0	0.1	1.51702	0.694245	1.461	0.676
0	0.2	1.54463	0.673566	1.463	0.658
0	0.5	1.7854	0.488086	1.469	0.616
0	5	1.47941	0.868859	1.647	0.420
0	10	1.800	0.410252	1.838	0.421
0	20	2.15426	0.556954	2.154	0.544

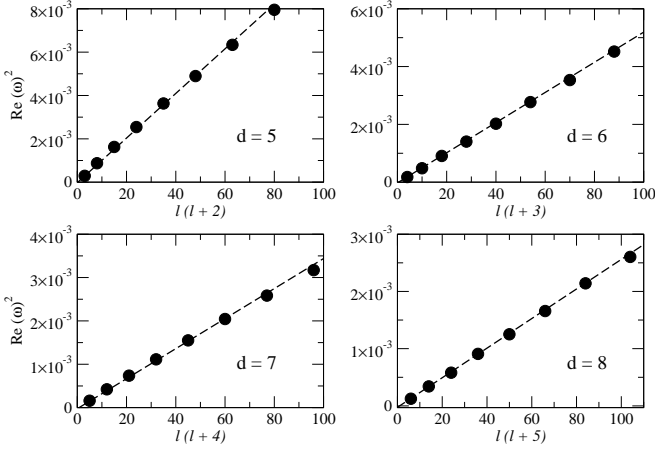


Figure 3: Graph of $\text{Re}(\omega)^2$ as a function of $\ell(\ell+d-3)$, in the near-extreme limit. The bullets are the values calculated from the time-evolution profiles, and the dashed lines are values obtained from the expression (16). The parameters in this graph are $\kappa_+ = 0.01$, $\alpha = 1$, $\mu = 1.0$.

ing. Yet, real part of ω is more sensitive to the changes of Λ -term. Qualitatively, this resembles the quasinormal oscillations of d -dimensional Schwarzschild-de Sitter black hole [21]. In the limit of extremal value of the Λ -term, i.e. when the cosmological horizon (r_c) is very close to the event horizon (r_+), it is possible to generalize the formulas found in [22] for four dimensional black hole and in [23] for d -dimensional case. Namely, the quasinormal frequencies are given by

$$\frac{\omega}{\kappa_+} = \sqrt{\frac{\ell(\ell+d-3)}{r_+^2} \frac{r_c - r_+}{2\kappa_+} - \frac{1}{4}} - i \left(n + \frac{1}{2} \right). \quad (16)$$

See Fig.3 for a comparison of the values obtained by direct numerical calculation and from Eq. (16). Thus the quasinormal modes are proportional to the surface gravity κ_+ , at least for lower overtones. It should be pointed that for the usual Schwarzschild-de Sitter black holes, numerical and analytical investigations [24] suggest that the high overtone behavior does not obey the formula (16).

When the mass parameter μ is set to zero, we have the case of pure de Sitter space-time in the Gauss-Bonnet gravity. The metric function (4) then reduces to the following form:

$$h(r) = 1 + \frac{r^2}{2\alpha} - \frac{r^2}{2\alpha} \sqrt{1 + \frac{8\alpha\Lambda}{(d-1)(d-2)}}. \quad (17)$$

Repeating the analysis of [25, 26], we come to the conclusion that quasinormal modes exist only in odd space-time dimensions and are given by the formula:

$$\omega_n = i \left[\frac{1}{2\alpha} \left(1 - \sqrt{1 + \frac{8\alpha\Lambda}{(d-1)(d-2)}} \right) \right]^{1/2} (2n + \ell) \quad (18)$$

$n = 0, 1, 2, \dots$

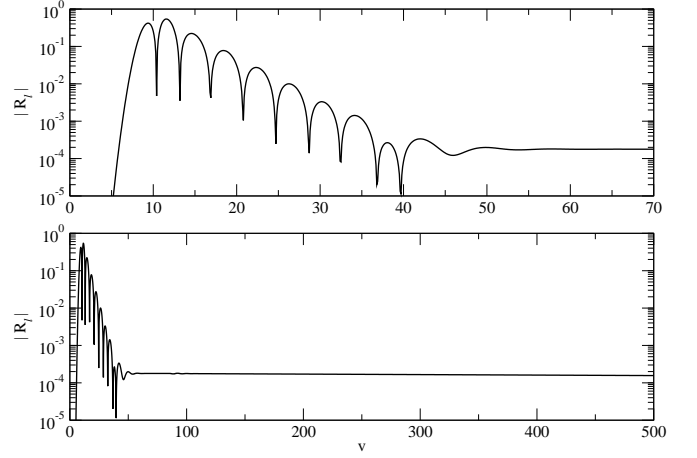


Figure 4: Field decay in the Gauss-Bonnet-de Sitter black holes, with $\ell = 0$. (above) A quasinormal mode dominated region is observed. (below) Asymptotically, the field decays to a constant. The fundamental mode, calculated with the WKB method and directly from the characteristic data are $0.8356 - 0.2935i$ and $0.8011 - 0.2608i$. The parameters in this graph are $d = 6$, $\alpha = 3.0$, $\Lambda = 0.1$ and $\mu = 1.0$.

Note that pure Gauss-Bonnet-de Sitter quasinormal modes are purely imaginary, which corresponds to exponential decaying without oscillations.

For the zero multipole field ($\ell = 0$), the time domain picture is the following: after a transient part, a quasinormal mode dominated region is best observed. Following the quasinormal mode dominated region, a late-time decay region settles. In this latter phase, the wave-functions decay asymptotically to a constant value, as has been the case in the Schwarzschild de Sitter black hole we studied before [16, 17, 27]. This is illustrated in Fig.4.

For first and higher multipoles ($\ell > 0$) at late times we observe exponential tails in vicinity of GBdS black hole. This is also an expected result, since in Einstein gravity the exponential tails are observed as well in usual de Sitter black holes [16, 17, 27]. This is illustrated in Fig.5.

The numerical simulations developed for Gauss-Bonnet-de Sitter black hole show a transition mechanism (between oscillatory modes and exponentially decaying modes) similar to the one found in the Schwarzschild-de Sitter black holes [27]. As the cosmological constant increases, the absolute value of $-\text{Im}(\omega_0)$ decreases. Above a certain critical value of Λ it is not observed the exponential tail ($\propto \exp(-k_{exp}t)$). This happens because the coefficient k_{exp} is larger than $-\text{Im}(\omega_0)$ thus the decaying quasinormal mode dominates. But for Λ smaller than this critical value, $-\text{Im}(\omega_0)$ turns out to be larger than k_{exp} and the exponential tail dominates the late time decay.

Table V: Values for the quasinormal frequencies for the fundamental mode in the Gauss-Bonnet-de Sitter geometry, obtained from third and sixth order WKB method, for $d = 5$, $\ell = 0$ and several values of α and Λ .

$d = 5$		WKB (3th order)		WKB (6th order)	
α	Λ	$\text{Re}(\omega_0)$	$-\text{Im}(\omega_0)$	$\text{Re}(\omega_0)$	$-\text{Im}(\omega_0)$
0.1	1/8	0.30485	0.278407	0.334981	0.26202
0.1	1/2	0.14922	0.217542	0.152444	0.2164
0.1	2/3	0.0677006	0.14792	0.00666957	0.150988
1	1/5	0.301869	0.218752	0.378865	0.159611
1	1	0.112613	0.148749	0.11619	0.145465
1	7/5	0.0240051	0.0683652	0.0242716	0.0709775

Table VI: Values for the quasinormal frequencies for the fundamental mode in the Gauss-Bonnet-de Sitter geometry, obtained from third and sixth order WKB method, for $d = 6$, $\ell = 0$ and several values of α and Λ .

$d = 6$		WKB (3th order)		WKB (6th order)	
α	Λ	$\text{Re}(\omega_0)$	$-\text{Im}(\omega_0)$	$\text{Re}(\omega_0)$	$-\text{Im}(\omega_0)$
0.1	1/4	0.580472	0.428367	0.652079	0.411337
0.1	1	0.379931	0.392027	0.401925	0.384688
0.1	2	0.0653851	0.168544	0.0636328	0.173794
1	1/2	0.582293	0.358225	0.736989	0.235326
1	2	0.318697	0.307084	0.331268	0.282461
1	4	0.00390515	0.0487306	0.0574555	0.0529852
10	100	1.5033	0.574511	1.5741	0.599309

Table VII: Values for the quasinormal frequencies for the fundamental mode in the Gauss-Bonnet-de Sitter geometry, obtained from third and sixth order WKB method, for $d = 7$, $\ell = 0$ and several values of α and Λ .

$d = 7$		WKB (3th order)		WKB (6th order)	
α	Λ	$\text{Re}(\omega_0)$	$-\text{Im}(\omega_0)$	$\text{Re}(\omega_0)$	$-\text{Im}(\omega_0)$
0.1	1	0.769109	0.556647	0.852395	0.551612
0.1	1	0.561644	0.517639	0.598484	0.511069
0.1	1	0.00963007	0.222564	0.0939457	0.228191
1	1	0.868246	0.48557	1.12603	0.2999562
1	4	0.461426	0.419016	0.483098	0.381285
1	7	0.113334	0.215329	0.111663	0.218394

Table VIII: Values for the quasinormal frequencies for the fundamental mode in the Gauss-Bonnet-de Sitter geometry, obtained from third and sixth order WKB method, for $d = 8$, $\ell = 0$ and several values of α and Λ .

$d = 8$		WKB (3th order)		WKB (6th order)	
α	Λ	$\text{Re}(\omega_0)$	$-\text{Im}(\omega_0)$	$\text{Re}(\omega_0)$	$-\text{Im}(\omega_0)$
0.1	1	1.1449	0.669364	1.29739	0.695376
0.1	4	0.644892	0.598472	0.682218	0.594199

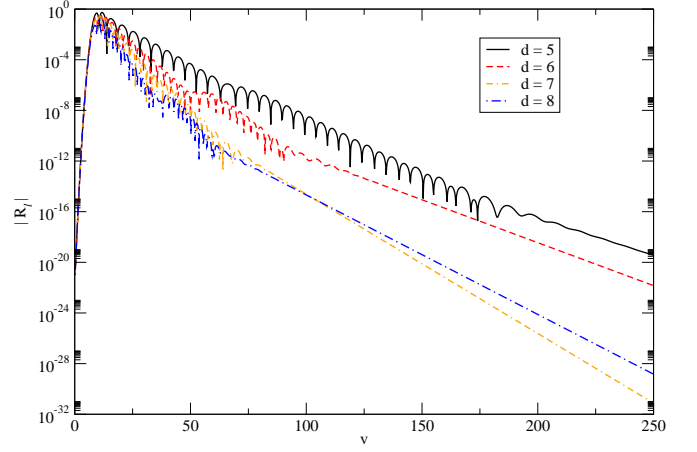


Figure 5: Field decay in the Gauss-Bonnet black holes, for $d = 5, 6, 7, 8$. It is observed a quasinormal mode dominated region. Asymptotically, the field decays as an exponential tail. The parameters in this graph are $\alpha = 0.1$, $\mu = 1.0$ and $\ell = 0$.

Table IX: Values for the quasinormal frequencies for the fundamental mode in the Gauss-Bonnet-de Sitter geometry, obtained from third and sixth order WKB method and directly from characteristic data, for $d = 5$, $\ell = 1$ and several values of α and Λ .

$d = 5$		WKB (6th order)		Characteristic Integration	
α	Λ	$\text{Re}(\omega_0)$	$-\text{Im}(\omega_0)$	$\text{Re}(\omega_0)$	$-\text{Im}(\omega_0)$
0.1	1/8	0.64317	0.241723	0.6451	0.2382
0.1	1/2	0.379265	0.165101	0.3856	0.1564
0.1	2/3	0.231024	0.103394	0.2247	0.1051
1	1/5	0.698655	0.181854	0.6926	0.1877
1	1	0.365998	0.111668	0.3704	0.1133
1	7/5	0.153506	0.0465747	0.1518	-0.042631

Table X: Values for the quasinormal frequencies for the fundamental mode in the Gauss-Bonnet-de Sitter geometry, obtained from third and sixth order WKB method and directly from characteristic data, for $d = 6$, $\ell = 1$ and several values of α and Λ .

$d = 6$		WKB (6th order)		Characteristic Integration	
α	Λ	$\text{Re}(\omega_0)$	$-\text{Im}(\omega_0)$	$\text{Re}(\omega_0)$	$-\text{Im}(\omega_0)$
0.1	1/4	1.04698	0.39859	1.0574	0.3828
0.1	1	0.74644	0.323514	0.7479	0.3183
0.1	2	0.238066	0.114496	0.2387	0.1212
1	1/2	1.09756	0.301244	1.053	0.2948
1	2	0.6962	0.244326	0.6962	0.2307
1	4	0.0847573	0.0315107	0.08965	0.03323
10	100	3.21004	0.52559	3.1940	0.5360
10	2000	-	-	2.1711	0.4900
10	5000	-	-	0.6228	0.2018

Table XI: Values for the quasinormal frequencies for the fundamental mode in the Gauss-Bonnet-de Sitter geometry, obtained from third and sixth order WKB method and directly from characteristic data, for $d = 7$, $\ell = 1$, $\alpha = 0.1$ and several values of Λ .

$d = 7$		WKB (6th order)		Characteristic Integration	
α	Λ	$\text{Re}(\omega_0)$	$-\text{Im}(\omega_0)$	$\text{Re}(\omega_0)$	$-\text{Im}(\omega_0)$
0.1	1	1.28621	0.519229	1.304	0.4910
0.1	2	1.00125	0.440876	1.008	0.4306
0.1	4	0.303405	0.153651	0.3091	0.1416
1	1	1.48546	0.411346	1.467	0.3623
1	4	0.899964	0.338928	0.8944	0.3224
1	7	0.361602	0.152214	0.3638	0.1398

Table XII: Values for the quasinormal frequencies for the fundamental mode in the Gauss-Bonnet-de Sitter geometry, obtained from third and sixth order WKB method and directly from characteristic data, for $d = 8$, $\ell = 1$, $\alpha = 0.1$ and several values of Λ .

$d = 8$		WKB (6th order)		Characteristic Integration	
α	Λ	$\text{Re}(\omega_0)$	$-\text{Im}(\omega_0)$	$\text{Re}(\omega_0)$	$-\text{Im}(\omega_0)$
0.1	1	1.75036	0.697491	1.803	0.6250
0.1	4	1.10954	0.508301	1.103	0.4964

C. Gauss-Bonnet-anti-de Sitter black holes

The quasinormal and late-time behavior of black holes in anti-de Sitter space-time is significantly different from those in asymptotically de Sitter or flat space-times. The key difference is stipulated by the effective potential behavior, which is divergent at spacial infinity. Thus the anti-de Sitter space acts as an effective confining box. In the usual Schwarzschild-anti-de Sitter black holes, they govern the decay at all times and thereby no power-law or exponential tails appear [18, 19]. We observe a similar behavior the scalar field perturbations in the Gauss-Bonnet-anti-de Sitter black holes.

It is not possible to use WKB method to find the quasinormal modes in Gauss-Bonnet-AdS case because the effective potential is not a potential barrier anymore. The Horowitz-Hubeny method [9] is not applicable either, because the Taylor expansion of the effective potential has infinite number of terms. That is why we were limited only by time domain analysis, which is free of the above problems. From Fig.6 we see that, indeed, the quasinormal modes are dominating even at sufficiently late times. We also observe that, as the multipole index ℓ grows, the quasinormal mode dominated region grows. This is illustrated in Fig. 6.

As is known from Einstein action case, as the radius of the AdS black hole goes to zero, the quasinormal modes of the black hole approach its pure anti-de Sitter values [28]. Repeating the calculations of [26], we find the exact

Table XIII: Values for the quasinormal frequencies for the fundamental mode in the Gauss-Bonnet-anti-de Sitter geometry, estimated from the characteristic data, for $d = 5$, $\ell = 0$, $\mu = 1.0$, $\Lambda = -0.1$ and several values of α .

α	$\text{Re}(\omega_0)$	$-\text{Im}(\omega_0)$
0.1	0.4923	-0.01585
0.1	0.4920	-0.01593
0.5	0.4904	-0.01634
1.0	0.4885	-0.01702
1.5	0.4866	-0.01766

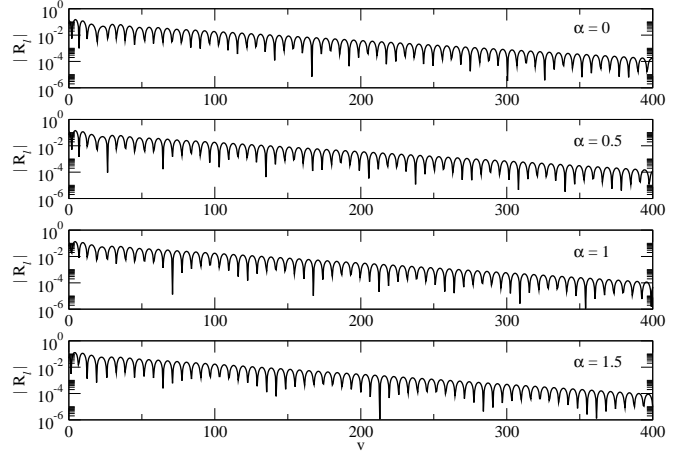


Figure 6: Field decay in the Gauss-Bonnet anti-de Sitter black holes, for several values of the Gauss-Bonnet coupling. It is observed a quasinormal mode dominated region. Asymptotically, the field decays in quasinormal modes. The parameters in this graph are $d = 5$, $\mu = 1.0$, $\Lambda = -0.1$ and $\ell = 0$.

expression for the normal modes in GB gravity:

$$\omega_n = \left[\frac{1}{2\alpha} \left(1 - \sqrt{1 + \frac{8\alpha\Lambda}{(d-1)(d-2)}} \right) \right]^{1/2} (2n + \ell + d - 1) \quad (19)$$

$n = 0, 1, 2, \dots$

The pure GB-AdS modes, unlike GB-dS modes, exist in any any space-time dimension.

Even though it is physically expected, it is difficult to check numerically with sufficient accuracy that the quasinormal modes of GBAdS black holes approach their pure GBAdS values when the radius of the black holes goes to zero.

V. CONCLUSIONS

We have considered here frequency and time domain description of evolution of scalar field perturbations in the exterior of black holes in Gauss-Bonnet theory of

gravity, generally with a Λ -term. The quasinormal behavior even though being corrected by a new parameter, Gauss-Bonnet coupling α , are qualitatively dependent mainly on the Λ -term and black hole parameters such as mass μ and multipole number ℓ . The late-time tails for asymptotically flat Gauss-Bonnet black holes, quite remarkably, do not depend on the Gauss-Bonnet coupling.

Even though our analysis can easily be extended to the massive scalar field, we were limited here by the massless case. We expect that the influence of the massive term upon the QNMs will be similar to that found in [29], i.e. the lower overtones should be corrected by the field mass, infinitely high overtone asymptotic will be unchanged no

matter the value of the massive term. Generally the high overtone asymptotics must be studied by totally different methods and deserves separate investigation [30].

Acknowledgments

This work was partially supported by *Fundação de Amparo à Pesquisa do Estado de São Paulo (FAPESP)* and *Conselho Nacional de Desenvolvimento Científico e Tecnológico (CNPq)*, Brazil.

-
- [1] L. Randall and R. Sundrum, Phys. Rev. Lett. **83** 3370, 4690 (1999).
 - [2] D. G. Boulware and S. Deser, Phys. Rev. Lett. **55**, 2656 (1985).
 - [3] J. Wheeler, Nucl. Phys. **B268**, 737 (1986).
 - [4] D. Lovelock, J. Math. Phys. **12**, 498 (1971).
 - [5] J. Crisostomo, R. Troncoso and J. Zanelli, Phys. Rev. D **62**, 084013 (2000).
 - [6] Elcio Abdalla and L. Alejandro Correa-Borbonet, Phys. Rev. D **65**, 124011 (2002).
 - [7] K. D. Kokkotas and B. G. Schmidt, Living Rev. Relativity **2**, 2 (1999).
 - [8] S. Nojiri, S. D. Odintsov, J. of High Energy Phys. **0007**, 049 (2000).
 - [9] G. T. Horowitz and V. E. Hubeny, Phys. Rev. D **62**, 024027 (2000); A. Nunez, A. O. Starinets, Phys. Rev. D **67**, 124013 (2003).
 - [10] R. Konoplya, Phys. Rev. D **71**, 024038 (2005).
 - [11] B. F. Schutz and C. M. Will, Astrophys. J. **291**, L33 (1985); S. Iyer and C. M. Will, Phys. Rev. D **35**, 3621 (1987); R. A. Konoplya, Phys. Rev. D **68**, 024018 (2003).
 - [12] S.K. Chakrabarti, K. S. Gupta. SINP-TNP-05-07, hep-th/0506133.
 - [13] G. Dotti, R. J. Gleiser, gr-qc/0503117.
 - [14] C. Gundlach, R. Price and J. Pullin, Phys. Rev. D **49**, 883 (1994).
 - [15] R. Price, Phys. Rev. D **5**, 2419 (1972).
 - [16] P. R. Brady, C. M. Chambers, W. Krivan and P. Laguna, Phys. Rev. D **55**, 7538 (1997).
 - [17] P. R. Brady, C. M. Chambers, W. G. Laarakkers and E. Poisson, Phys. Rev. D **60**, 064003 (1999).
 - [18] B. Wang, C. Molina and E. Abdalla, Phys. Rev. D **63**, 084001 (2001).
 - [19] Bin Wang, Chi-Yong Lin, C. Molina, Phys. Rev. D **70**, 064025 (2004).
 - [20] E. Berti, K. D. Kokkotas, Phys. Rev. D **71**, 124008 (2005); R. A. Konoplya, Phys. Rev. D **66**, 084007 (2002); S. Fernando, Gen. Rel. Grav. **37** 585 (2005); R. A. Konoplya, E. Abdalla, Phys. Rev. D **71**, 084015 (2005); R. A. Konoplya, C. Molina Phys. Rev. D **71**, 124009 (2005); H. Nomura, T. Tamaki, Phys. Rev. D **71**, 124033 (2005).
 - [21] R. A. Konoplya, Phys. Rev. D **68**, 124017 (2003).
 - [22] V. Cardoso and J. P. S. Lemos, Phys. Rev. D **67** 084020 (2003).
 - [23] C. Molina, Phys. Rev. D **69** (2004) 104013.
 - [24] V. Cardoso, J. Natario, R. Schiappa, J. Math. Phys. **45** 4698 (2004); R. A. Konoplya and A. Zhidenko, JHEP (06) 037 (2004).
 - [25] E. Abdalla, K. H. C. Castello-Branco, A. Lima-Santos, Phys. Rev. D **66**, 104018 (2002).
 - [26] J. Natario, R. Schiappa, hep-th/0411267 (to be published in Adv. Theor. Math. Phys.).
 - [27] C. Molina, D. Giugno, E. Abdalla, A. Saa, Phys. Rev. D **69** (2004) 104013.
 - [28] R. A. Konoplya, Phys. Rev. D **66**, 044009 (2002).
 - [29] R. A. Konoplya, Phys. Lett. **B 550**, 117 (2002); R. A. Konoplya, A. V. Zhidenko, Phys. Lett. **B 609**, 377 (2005).
 - [30] S. K. Chakrabarti, K. S. Gupta, hep-th/0506133.